

Supporting information

Near Infrared Light Activatable PEI-Wrapped Bismuth Selenide Nanocomposites for Photothermal/Photodynamic Therapy Induced Bacterial Inactivation and Dye Degradation

Govinda Gorle^a, Ayyappa Bathinapatla^a, Yi-Zhan Chen^a, and Yong-Chien Ling^{a*}

^a Department of Chemistry, National Tsing Hua University, Hsinchu 30013, Taiwan.

*Corresponding author: ycling@mx.nthu.edu.tw

Materials

Analytical grade bismuth (III) nitrate pentahydrate ($\text{Bi}(\text{NO}_3)_3 \cdot 5\text{H}_2\text{O}$) (98%), sodium selenite pentahydrate ($\text{Na}_2\text{SeO}_3 \cdot 5\text{H}_2\text{O}$) (99%), ethylene glycol, isopropyl alcohol, ethanol, 1,3-Diphenylisobenzofuran (DPBF), 4',6-Diamidino-2-phenylindole dihydrochloride (DAPI), polyethyleneimine (PEI), propidium iodide (PI), methylene blue (MB), Rhodamine B (RhB), phosphate-buffered saline (PBS) solution and agar powder were purchased from Sigma-Aldrich.

Characterization

The as-prepared Bi_2Se_3 NPs and Bi_2Se_3 NPs/PEI were characterized as follows. The crystal structures of the samples were analyzed by powder X-ray diffraction (XRD) on a Rigaku D/MAX-2500 X-ray diffractometer with $\text{Cu K}\alpha$ radiation ($\lambda = 1.5406 \text{ \AA}$) at 40 kV and 20 mA. The surface modification was characterized by FTIR spectroscopy. In this, Bi_2Se_3 NPs and Bi_2Se_3 NPs/PEI were dried and grounded with KBr and FTIR spectra were recorded by a Perkin-Elmer system 2000 FTIR spectrophotometer with a resolution of 2 cm^{-1} . The UV-Vis-NIR spectra were recorded using a JASCO V-570 spectrometer in the wavelength range from 350 to 1200 nm, with a resolution of 1 nm. The morphologies and elemental composition of the Bi_2Se_3 NPs were analyzed by a JEOL JEM-2100 TEM coupled with an EDXA analyzer as well as a JEOL, JSM-7000F SEM. The zeta potential was measured with a Nicomp 380 ZLS from Particle Sizing Systems.

Photothermal Conversion Efficiency of Bi_2Se_3 NPs/PEI

The photothermal conversion efficiency of the Bi_2Se_3 NPs/PEI NPs was calculated according to the reported methods.¹⁻³ Briefly, 80 ppm Bi_2Se_3 NPs/PEI ($\text{OD}_{808} = 1$) in a 1.7 mL centrifuge vial was irradiated with an 808 nm laser. The diameter of the laser beam was 1 cm, the power

density was 1 W/cm². A thermocouple was inserted into the solution to record the temperature. The temperature was monitored during both heating (laser on) and cooling (laser off) stages. The photothermal conversion efficiency η was calculated using the following equation,

$$\eta = \frac{hS(T_{max} - T_{amb}) - Q_{dis}}{I(1 - 10^{-A_{808}})} \quad \text{equation (1)}$$

where, h = heat transfer coefficient, S = surface area of the container, T_{max} = maximum equilibrium temperature, T_{amb} = ambient temperature of the surroundings, Q_{dis} = laser-induced heat input by the container, I = laser power, and A_{808} = absorbance of the NPs at 808 nm.

The same experiment was conducted with water as the control to determine Q_{dis} (mW) by

$$Q_{dis} = 10^3 \cdot m \cdot C \cdot \Delta T / t \quad \text{equation (2)}$$

where, m = mass of water (g), C = heat capacity of water (J g⁻¹ K⁻¹), ΔT = increased temperature (K), and t = laser exposure time (s).

The term hS was calculated based on

$$hS = \frac{\sum_i m_i C_{p,i}}{\tau_s} \quad \text{equation (3)}$$

where, τ_s = sample system time constant and i = system components (NP suspension and sample container).

τ_s is related to a dimensionless driving force temperature θ by

$$t = -\tau_s \ln \theta \quad \text{equation (4)}$$

where, t = cooling time and θ is given by

$$\theta = (T - T_{amb}) / (T_{max} - T_{amb}) \quad \text{equation (5)}$$

In these studies, the temperature of NPs solution under continuous laser irradiation and subsequent cooling after the laser being turned off was recorded. The cooling process was used to determine the rate of heat transfer from the NPs solution to the environment. The temperature increased by 56 °C, when the NPs solution was irradiated for 10 min and did not change significantly upon further irradiation. The temperature reached a maximum threshold value because of the equilibrium between the heat input and output. In contrast, the temperature of the control water increased by only 1.2 °C. Using eq. 2 and the heating profile of the water, the Q_{dis} was determined to be 2.51 mW. The thermal equilibrium time constant (τ_s) was measured from the plot of cooling time t versus the term $-\ln \theta$ which shows a linear relationship and gives a slope of 3.26 min. Using eq. 3, the term hS was calculated to be 6.43 mW/°C. On the basis of eq. 1, the efficiency of transducing the red laser to heat by the Bi₂Se₃ NPs/PEI NPs was calculated to be 32.07%.

Optimization of preparation conditions.

Effect of ethylene glycol: To study the effect of ethylene glycol (EG), the Bi_2Se_3 NPs were prepared in two high boiling solvents oleic acid (OA) and EG. The morphology of the obtained Bi_2Se_3 NPs was observed under a SEM. As shown in Fig. S12, only Bi_2Se_3 NPs prepared in EG exhibited definite morphology, indicating that EG serves as both solvent and structure-directing agent.

Effect of reaction time and temperature: The Bi_2Se_3 NPs were prepared under different reaction time and temperature and the morphology was observed under a SEM. The results indicate that the minimum reaction time and temperature to obtain definite structure is 5 h and 260 °C, respectively (Fig. S11).

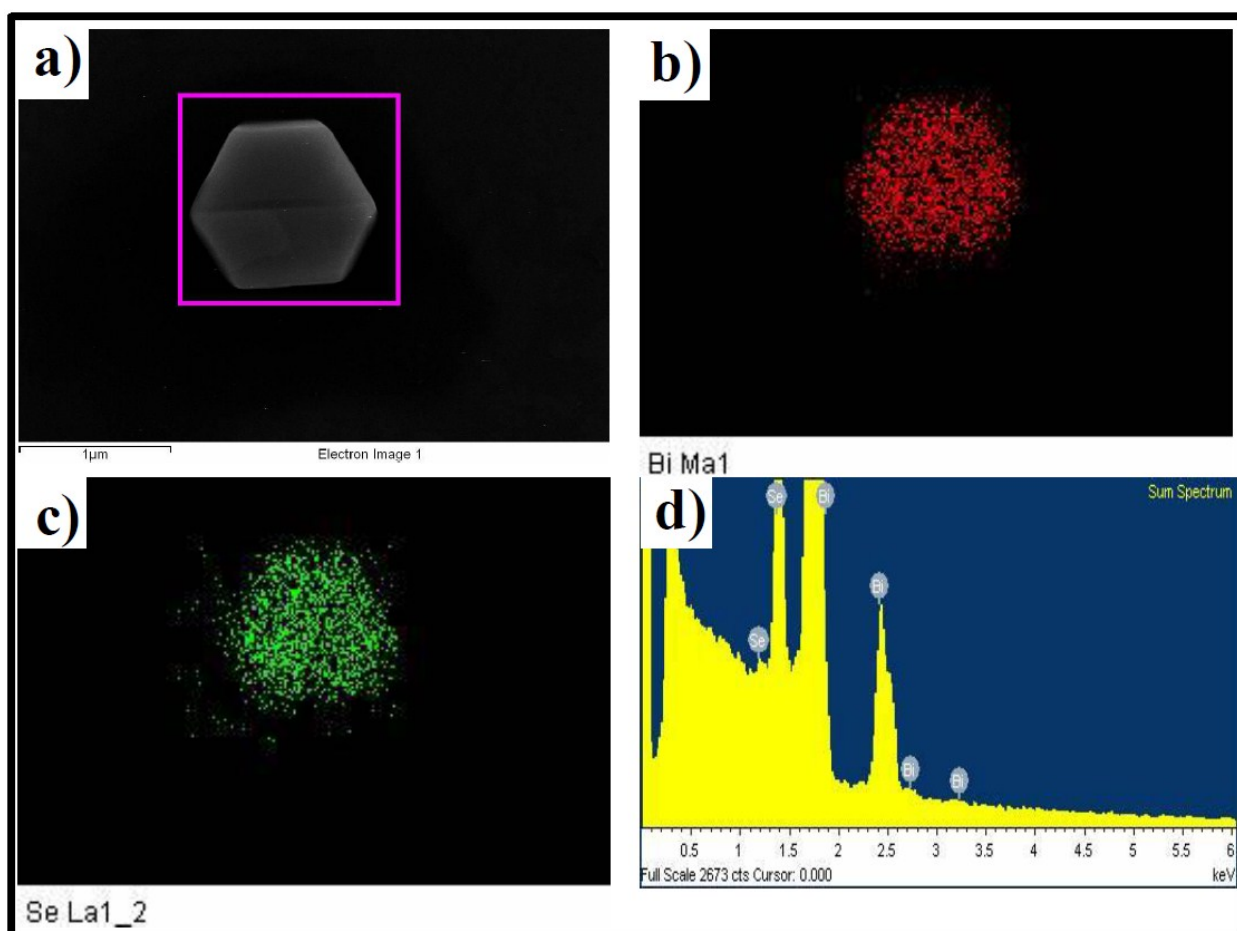


Fig. S1. Characterization of Bi_2Se_3 NPs: (a) SEM image, (b) EDXA mapping of bismuth, (c) EDXA mapping selenium, and (d) EDXA spectrum.

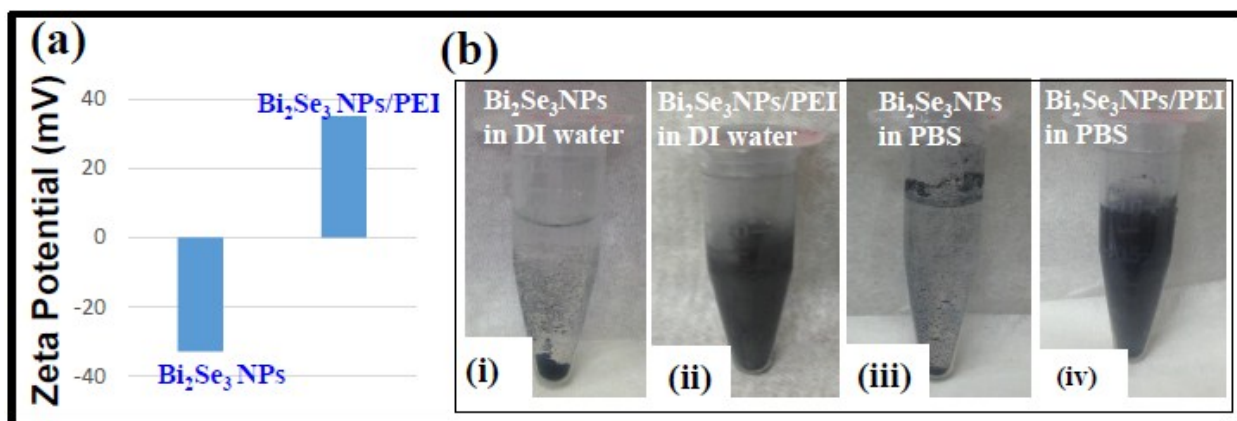


Fig. S2. Zeta potential values of Bi_2Se_3 NPs and Bi_2Se_3 NPs/PEI (a); the solution appearance of Bi_2Se_3 NP before (i, iii) and after (ii, iv) after PEI conjugation (b).

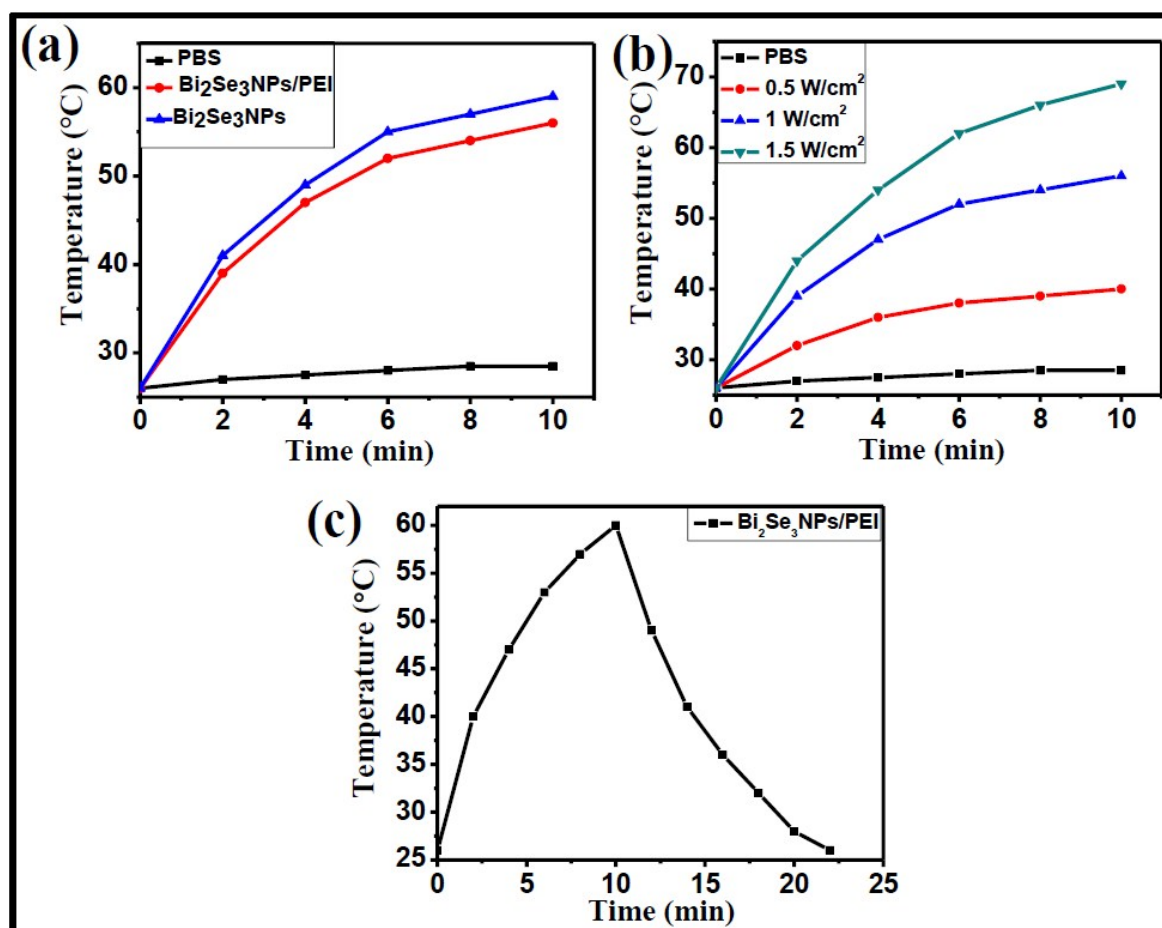


Fig. S3. Temperature elevation profile: (a) Temperature elevation profile of PBS, 80 ppm Bi_2Se_3 NPs, 80 ppm Bi_2Se_3 NPs/PEI (808 nm laser, 1 W/cm^2 , 10 min), (b) Temperature elevation profiles of Bi_2Se_3 NPs/PEI at different power densities (80 ppm, 808 nm), (c) Typical curves of the solution temperature of the Bi_2Se_3 NPs/PEI versus time in a procedure of laser-on for 10 min and then laser-off.

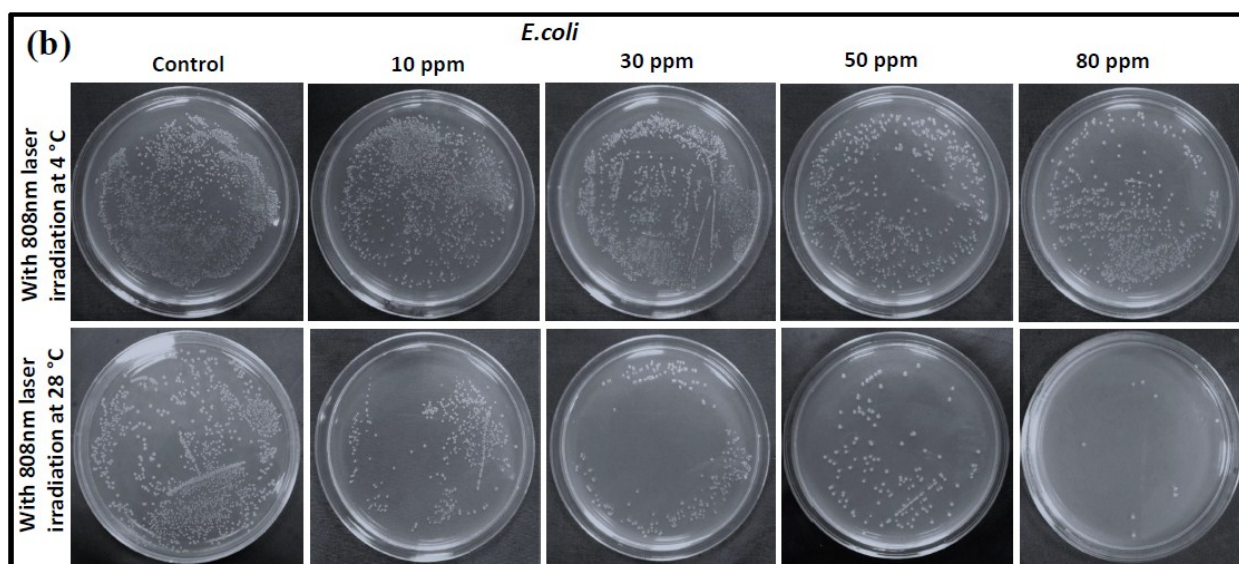
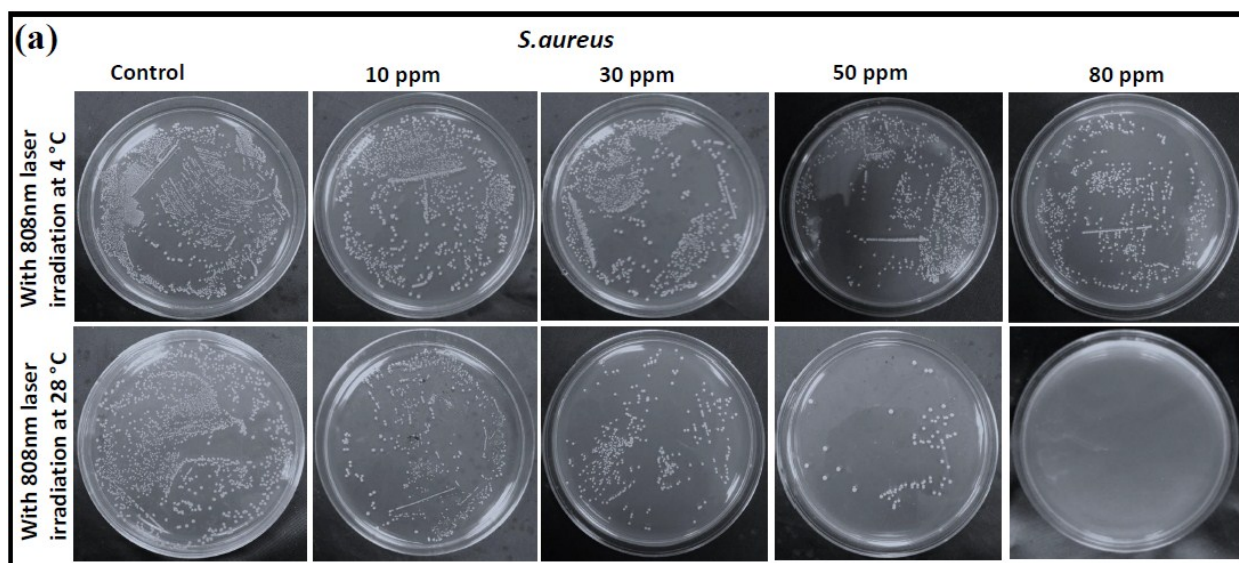


Fig. S4. Photographic images of *S. aureus*(a) and *E. coli*(b) viability at different conc. of Bi₂Se₃ NPs/PEI: with laser at 4 °C (1,3 rows), with laser at 28 °C (2,4 rows; 808 nm, 1W/cm², 10 min).

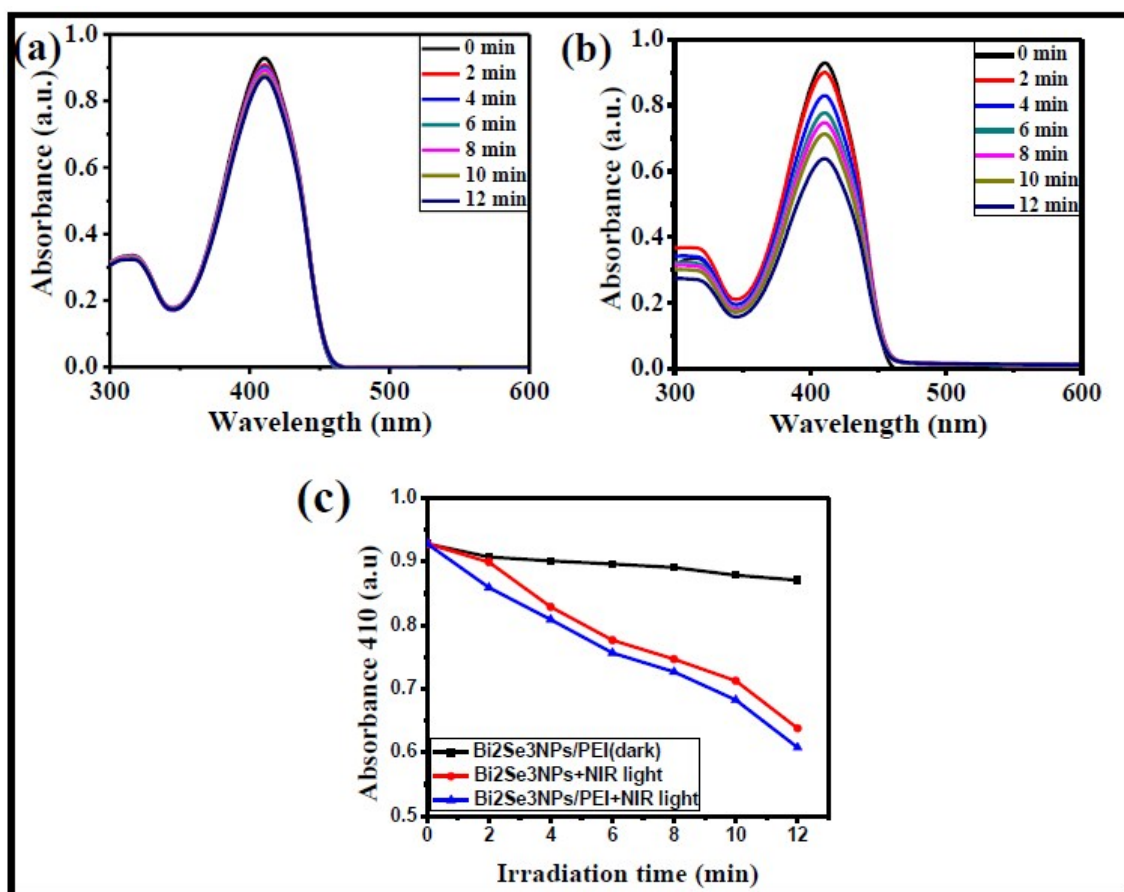


Fig. S5. Time dependent DPBF quenching experiment, (a) DPBF+ Bi₂Se₃/PEI(dark) (b) DPBF + NIR light+ Bi₂Se₃/PEI, and (c) Comparison of ¹O₂ generation efficiency between Bi₂Se₃ NPs and Bi₂Se₃ NPs/PEI upon NIR laser irradiation.

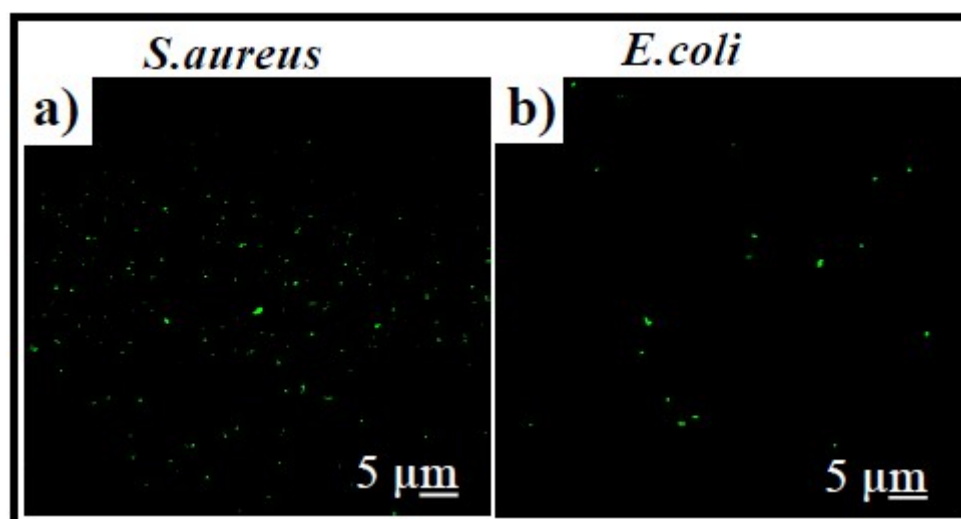


Fig. S6. Fluorescence microscopy (confocal) images showing the PDT cytotoxicity of *S. aureus* (a) and (b) *E. coli* after 10 min irradiation by an 808 nm NIR laser at 1 W/cm² with Bi₂Se₃ NPs/PEI by the detection of reactive oxygen species production inside the bacteria using DCFH-DA fluorescence probe.

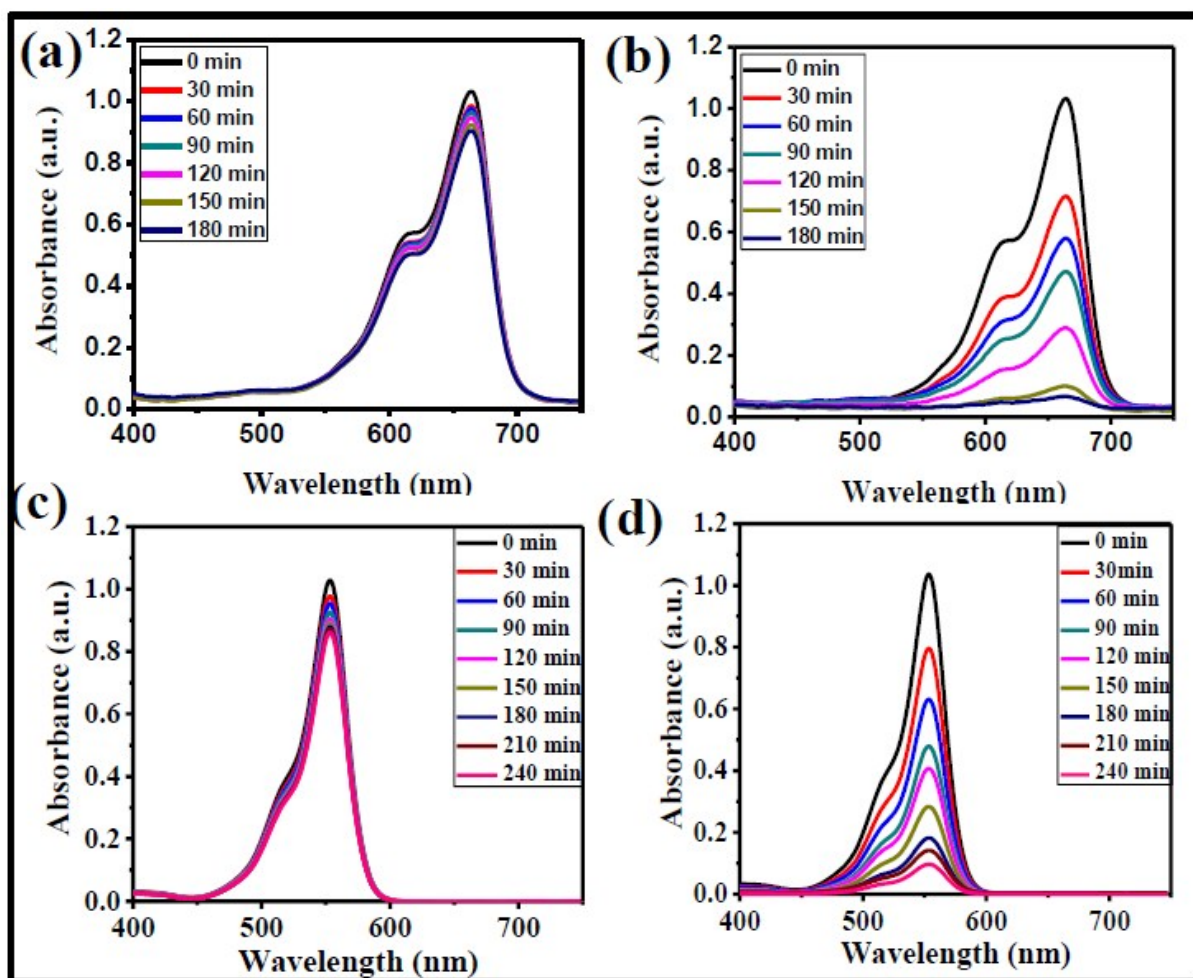


Fig. S7. Photocatalytic activity through photodegradation of MB under the experimental conditions (a) MB+Bi₂Se₃ NPs/PEI (in dark) and (c) MB+NIR light+Bi₂Se₃ NPs/PEI. Photocatalytic activity through photodegradation of RhB under the experimental conditions (c) RhB+ Bi₂Se₃ NPs/PEI (in dark) and (d) RhB+NIR light + Bi₂Se₃ NPs/PEI.

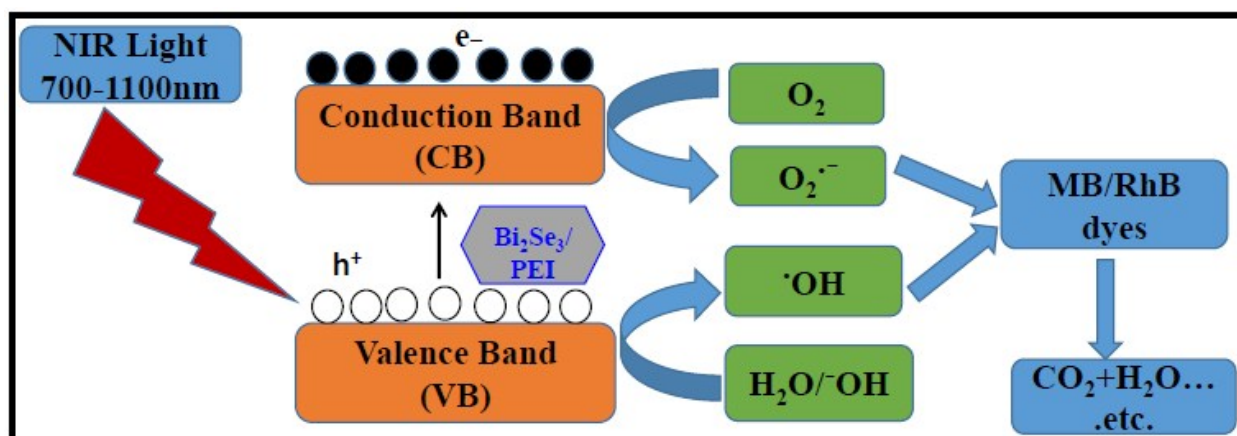


Fig. S8. Schematic of the charge transfer process for the photodegradation of MB and RhB dyes by Bi₂Se₃ NPs/PEI with NIR light.

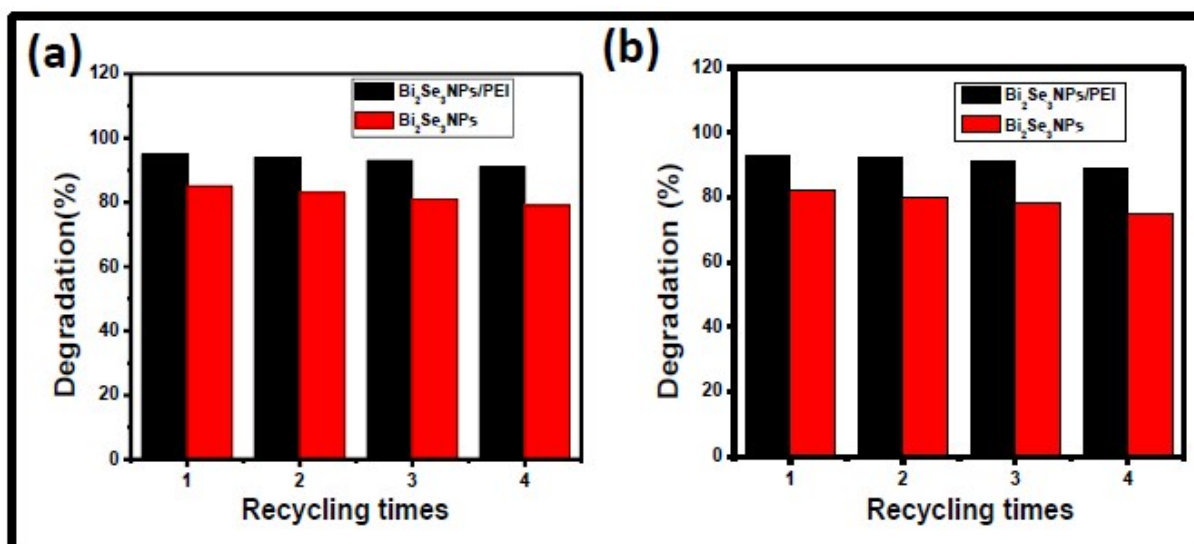


Fig. S9. The recycling experiments for photodegradation of (a) MB and (b) Rh B with Bi₂Se₃ NPs and Bi₂Se₃ NPs/PEI along with NIR light.

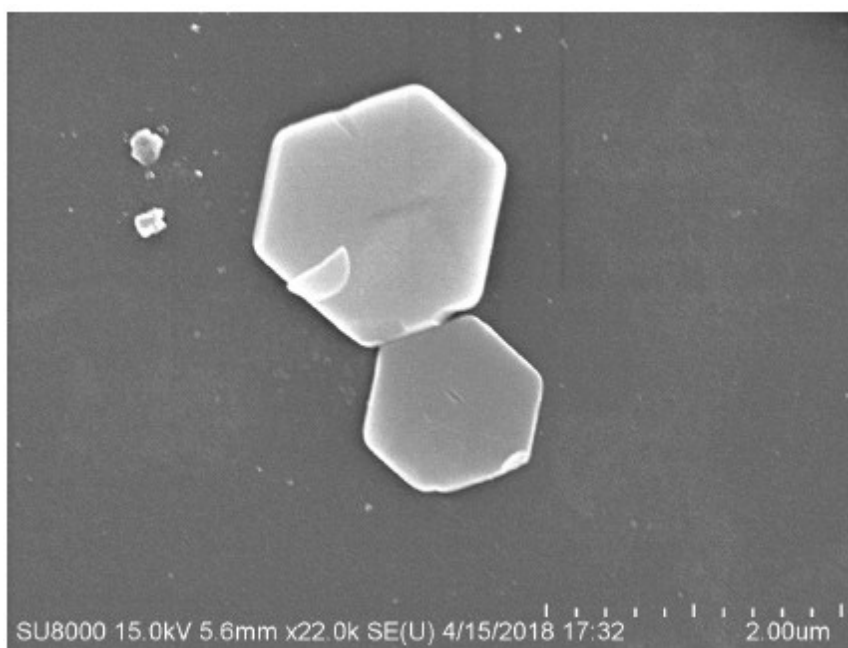


Fig. S10. The SEM images of recycle photocatalyst (Bi₂Se₃ NPs/PEI) upon photodegradation.

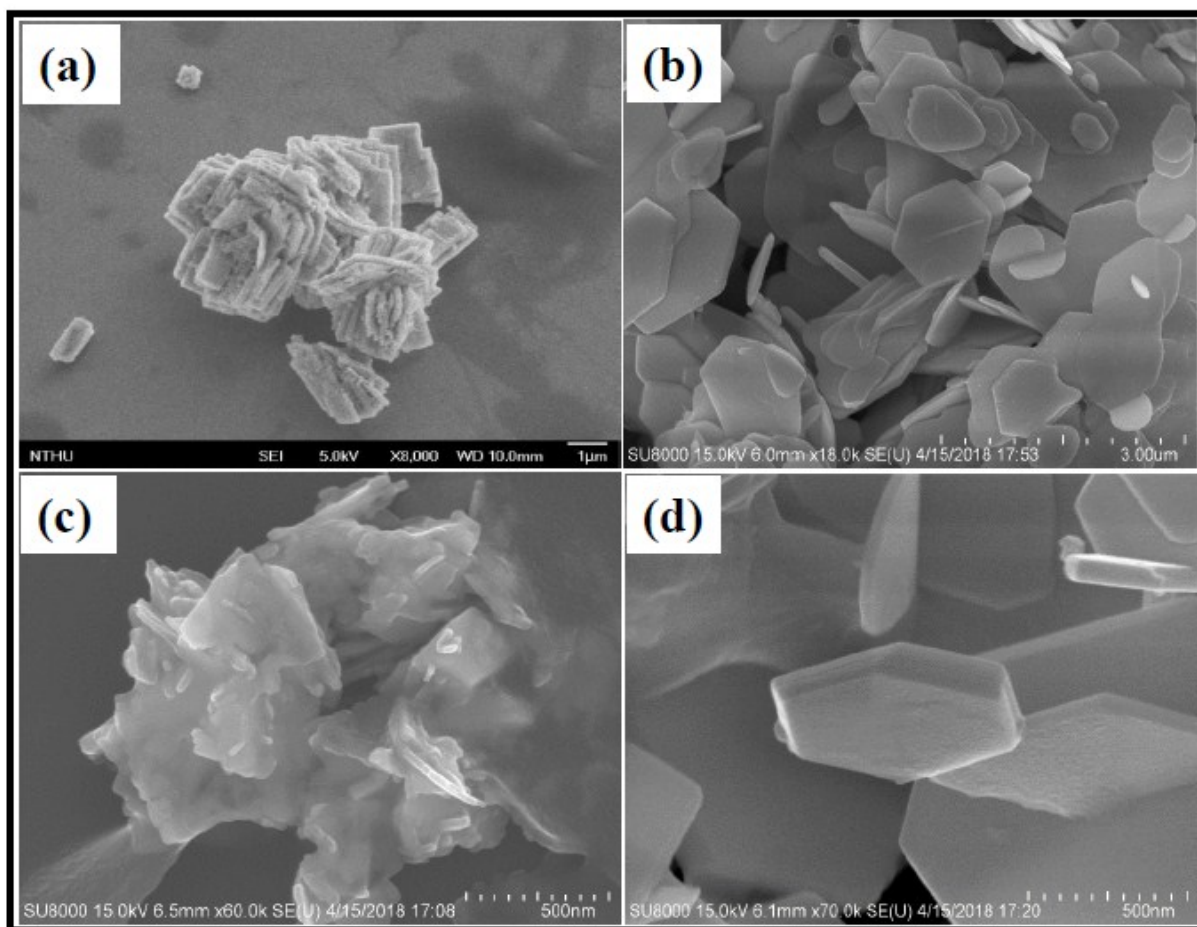


Fig. S11. SEM images of Bi₂Se₃ prepared under different time and temperature parameters: (a) at 200°C for 5 h, (b) at 300°C for 5 h, (c) at 260°C for 3 h, and (d) at 260°C for 7 h..

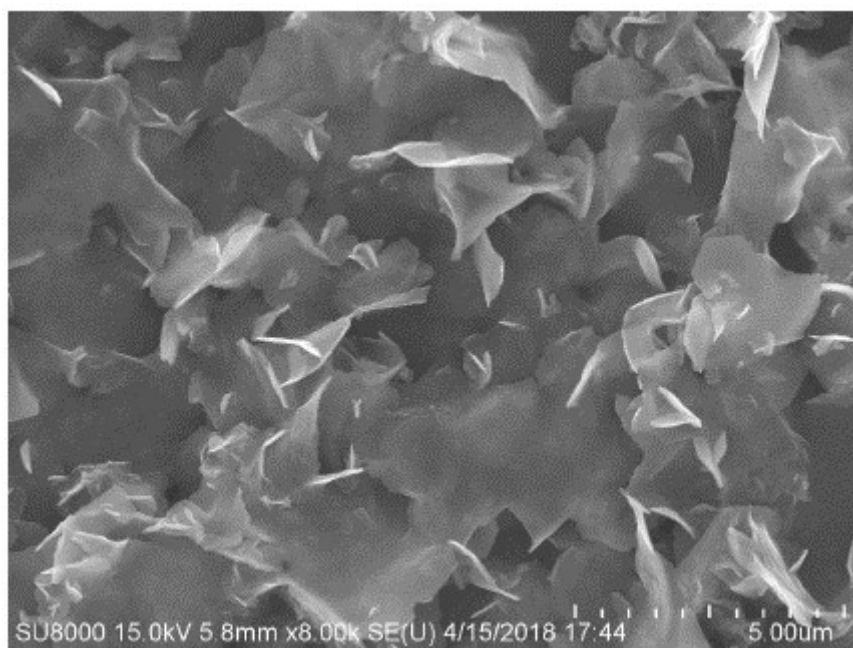


Fig. S12. SEM images of Bi₂Se₃ prepared using oleic acid as solvent at 260°C for 5 h.

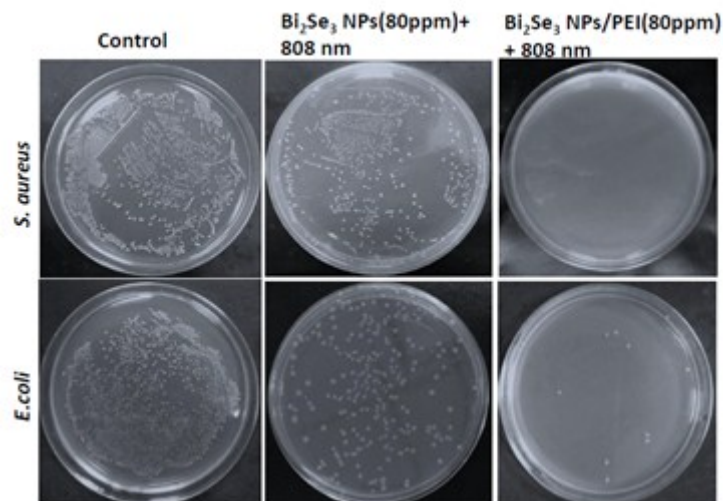


Fig. S13. Comparison of antibacterial activity between Bi_2Se_3 NPs and Bi_2Se_3 NPs/PEI at 80 ppm concentration upon NIR laser irradiation.

Table S1. Comparison of Bi_2Se_3 NPs/PEI with reported materials in terms of antibacterial activity.

Material	Laser nm	Power density W/cm^2	Concentration mg/mL	Time (min)	Killing g% (~)	Ref
MGO	808	1.5	0.08	10	100	4
PVPS: PANI	808	2	1-5	5	100	5
Graphene sheets	808	7.5	0.06-5	10	100	6
Fe_3O_4 @PEDOT	808	2	0.01-1	7	100	7
PPy- SiO_2	808	1.5	0.025-0.2	10	100	8
Bi_2Se_3 NPs/PEI	808	1	0.01-0.08	10	100	Present work

Table S2. Comparison of Bi₂Se₃NPs/PEI with reported materials in terms of photo degradation capacity

Material	Light	Irradiation time (h)	Concentration mg/mL	No of Cycles	Ref
ZnO/Au NPs	UV	1.1	0.4	NA	9
Zn/ CdS NSs	UV	4	1	4	10
BiOCl-PT	UV	3	30	NA	11
BiVO ₄ materials	Visible	2	5	NA	12
NaYF ₄ :Yb, Tm@TiO ₂ CSNPs	NIR	14	1	NA	13
Bismuth NSs	Visible	9.5	0.40	NA	14
GO-Ag ₃ PO ₄	Visible	3	20	4	15
Bi ₂ Se ₃ NPs/PEI	NIR	3	0.25	4	Present work

References

- 1 S. Bhana, G. Lin, L. Wang, H. Starring, S. R. Mishra, G. Liu and X. Huang, *ACS Appl. Mater. Interfaces* 2015, **7**, 11637–11647.
- 2 J. Guozhi, W. Peng, Z. Yanbang and C. Kai, *Sci. Rep.*, 2016, **6**:25884, 1-8.
- 3 Z. Xiao, X. Jiang, B. Li, X. Liu, X. Huang, Y. Zhang, Q. Ren, J. Luo, Z. Qin and J. Hu, *Nanoscale*, 2015, **7**, 11962–11970.
- 4 M. C. Wu, A. R. Deokar, J. H. Liao, P. Y. Shih, and Y. C. Ling, *ACS Nano*, 2013, **7**, 1281–1290.
- 5 S. H. Kim, E. B. Kang, C. J. Jeong, S. Md. Sharker, I. In and S. Y. Park, *ACS Appl. Mater. Interfaces*, 2015, **7**, 15600–15606.
- 6 O. Akhavan, E. Ghaderi, and A. Esfandiari, *J. Phys. Chem. B*, 2011, **115**, 6279–6288.
- 7 C. J. Jeong, S. Md. Sharker, I. In, and S. Y. Park, *ACS Appl. Mater. Interfaces*, 2015, **7**, 9469–9478.
- 8 E. Ju, Z. Li, M. Li, K. Dong, J. Ren and X. Qu, *Chem. Comm.*, 2013, **49**, 9048-9050.

- 9 W. Xia, C. Mei, X. Zeng, G. Fan, J. Lu, X. Meng and X. Shen, *ACS Appl. Mater. Interfaces*, 2015, **7**, 11824–11832.
- 10 F. Yang, N. N. Yan, S. Huang, Q. Sun, L. Z. Zhang and Y. Yu, *J. Phys. Chem. C*, 2012, **116**, 9078–9084.
- 11 M. Guerrero, A. Altube, E. G. Lecina, E. Rossinyol, M. D. Baró, E. Pellicer and J. Sort, *ACS Appl. Mater. Interfaces*, 2014, **6**, 13994–14000.
- 12 T. Saison, N. Chemin, C. Chanéac, O. Durupthy, L. Mariey, F. Maugé, V. Brezová and J. P. Jolive, *J. Phys. Chem. C*, 2015, **119**, 12967–12977.
- 13 Y. Tang, W. Di, X. Zhai, R. Yang and W. Qin, *ACS Catal.* 2013, **3**, 405–412.
- 14 Z. Wang, C. Jiang, R. Huang, H. Peng and X. Tang, *J. Phys. Chem. C*, 2014, **118**, 1155–1160.
- 15 Y. Xu, S. Huang, H. Ji, L. Jing, M. He, H. Xu, Q. Zhang and H. Li, *RSC Adv.*, 2016, **6**, 6905–6914.